# Supplementary Information

***The cargo-binding domain regulates structure and activity of myosin 5***

Kavitha Thirumurugan, Takeshi Sakamoto, John A Hammer III,
James R. Sellers and Peter J. Knight

**This document contains:**

## 1 Supplementary Discussion

Some extra detail is given here that could not be fitted into the main text

**Comparison of electron micrograph images with molecular models** The comparisons between image averages and atomic models have been done by eye. For the following reasons, attempting to be more sophisticated would probably be less satisfactory. It should be appreciated that the construction of models depends on many assumptions about the true structure of the lever. To produce contacts between adjacent calmodulins we have chosen to construct a lever model that incorporates bends in the heavy chain α-helix between the light chain binding IQ motifs with 25 residue spacing, and straight α-helix where the spacing is 23 residues. However, there is both crystallographic and electron microscope evidence for variation in heavy chain bending between light chains and also within the IQ motif itself. Thus the lever has many points of flexibility, allowing it to adopt a shape that best accommodates its local environment. In the folded structure, the interactions of the motor domains with the GTDs and the forced juxtaposition of the two levers at the lever-tail junction will likely combine to bend the lever away from the structure it would commonly assume in an isolated head in a crystal. Thus it is impossible to construct a model *ab initio* that will fully match the structure of the folded molecule. Therefore attempts to obtain objective best fits between image averages and 2D projections of a particular head model will be compromised because the model used will be incorrect. In addition, in the folded molecule there are GTDs adjacent to the head, and it would be difficult to exclude them from the fitting. Finally, one would be trying to fit an atomic model against a negative stained outline of the head, which is a difficult comparison. For all these reasons, in the present study we make instead an experienced judgement of how well reasonable models of an isolated head fit the 2D image. In fitting by eye, we can give weight to (or ignore) selected parts of the models and image averages which would be very difficult by any projection matching algorithm. As it turns out, the structures and the differences between them are so well-marked that there is little chance of ambiguity.

**Conformation of the right head of folded myosin** Assignment of the left head to the post-rigor rather than pre-powerstroke conformation is clear from a comparison with the atomic models, but assignment of the right head is less easy. The right head overall better fits the pre-powerstroke model (Fig. 1n), largely because the lever in that model better fits the appearance seen, and lies in the plane of the page so it is easy to see how it could unite with the left lever at the lever-tail junction. By contrast, when the post-rigor model is oriented appropriately for the motor domain to resemble the image averages, the lever curves to the left and points out of the plane towards the viewer. However, the emergence point of the lever from the motor domain in the image averages better matches the post-rigor model, in that in the image averages the lever consistently emerges on the left side of the triangular motor domain rather than the lower apex. This suggests that the converter location in the right head matches the post-rigor position rather than the pre-powerstroke position. Flexibility within the lever of a post-rigor molecule could allow the lever to follow the path seen in the image averages rather than that seen in the post-rigor model (Fig. 1m), and this flexibility could contribute to the generally less well-defined appearance of the right lever in the image averages. Further evidence that the right head is not in the pre-powerstroke conformation comes from analysis of preliminary datasets of folded molecules prepared in the presence of ADP or no nucleotide, in which pre-powerstroke conformers should be rare. The class averages show a similar appearance of the right head to the main ATP dataset (Fig. 1h & i *cf* a-e).

**Assignment of GTD-binding region to Pro117-Pro137 of the motor domain** The shape of the left head motor domain in the image averages (Fig. 1a-e) is rather consistent between averages and closely resembles the appearance we have previously described in myosin 2, myosin 5 HMM and also the appearance of the motor domain in single myosin 5 heads (Fig. 1g). The shape resembles a human head seen in profile from the left side, with a prominent nose and dark eye socket. The features are well fitted by a particular projection of the atomic structure of the motor domain that is shown in Fig. 1l. The nose is then seen to correspond to the lower 50kDa segment of the structure, which shows that the actin binding site is on the upper left of the head in this view. The nucleotide-binding pocket is located towards the back of the head at the same level as the nose (as shown in Fig. 2a & b). The N-terminal SH3 domain forms the chin, and the converter domain forms the neck connecting to the proximal calmodulin of the lever (which is cyan in Fig. 2a). Comparison of the folded molecule averages with the single head average (Fig. 1g) shows an additional stain-excluding feature at the base of the skull, below the level of the nucleotide-binding pocket. This must be the GTD. Comparison with the atomic model is now straightforward, as the base of the skull appears to arise from a single segment of heavy chain, approximately comprising Pro117-Pro137, as shown in Fig. 2a & b. Contiguous with this segment is His138-Glu154 that forms helix E of the motor domain (seen roughly end-on in Fig. 2b), and which could possibly also contact the GTD. Above this segment (above spacefilled E121 in Fig. 2b) is a surface loop (commonly referred to as loop 1 in the myosin literature). This is level with the upper part of the nose, and therefore too high up on the head to interact with the GTD. Loop 1 is not sufficiently long to reach down to interact with the GTD. Although it may seem surprising that negative stain imaging can lead to identification of precise regions of interaction, we have previously achieved a similar precision in describing the binding of myosin heads on actin[1].

With regard to the GTD binding site on the right head, the approximately triangular right head motor domain is well matched by orienting the post-rigor model so that its motor domain is seen almost end on, with the converter towards the upper left corner and the SH3 domain at the lower corner. This view places Pro117-Pro137 just above the junction of the lever and motor domains. In the image averages, the GTD is seen above the lever and extending into the lever-motor junction, just as expected if it binds in the same way to the right motor domain as to the left. Note that because the right motor is almost end on, the lever-motor junction and the GTD binding site are held above the plane of the carbon film on which the molecule rests. This may account for the relatively weak stain exclusion of the GTD and the start of the lever in the images.

There are two allosteric routes by which binding of the GTD could perturb ATPase activity. First, the N-terminal part of Pro117-Pro137 interacts with the C-terminal turns of helix F of the motor domain (the horizontal helix in Fig. 2b). At the N-terminus of helix F is the P-loop, critical for ATPase activity, which could therefore be sensitive to GTD binding. Second, the residues upstream of Pro117, to Asn111, form part of the binding sites for the adenine and ribose moieties of ATP. GTD-binding could thus have a big effect on affinity for nucleotide. Pro117-Pro137 together with helix E (His138-Glu154) inserts between strands 2 and 4 of the 7-strand β-sheet that is the core of the motor domain. Binding of GTD could therefore modify the conformational plasticity of the sheet, inhibiting both tight actin binding and actin activation of the myosin ATPase.

## 2 Supplementary Figures

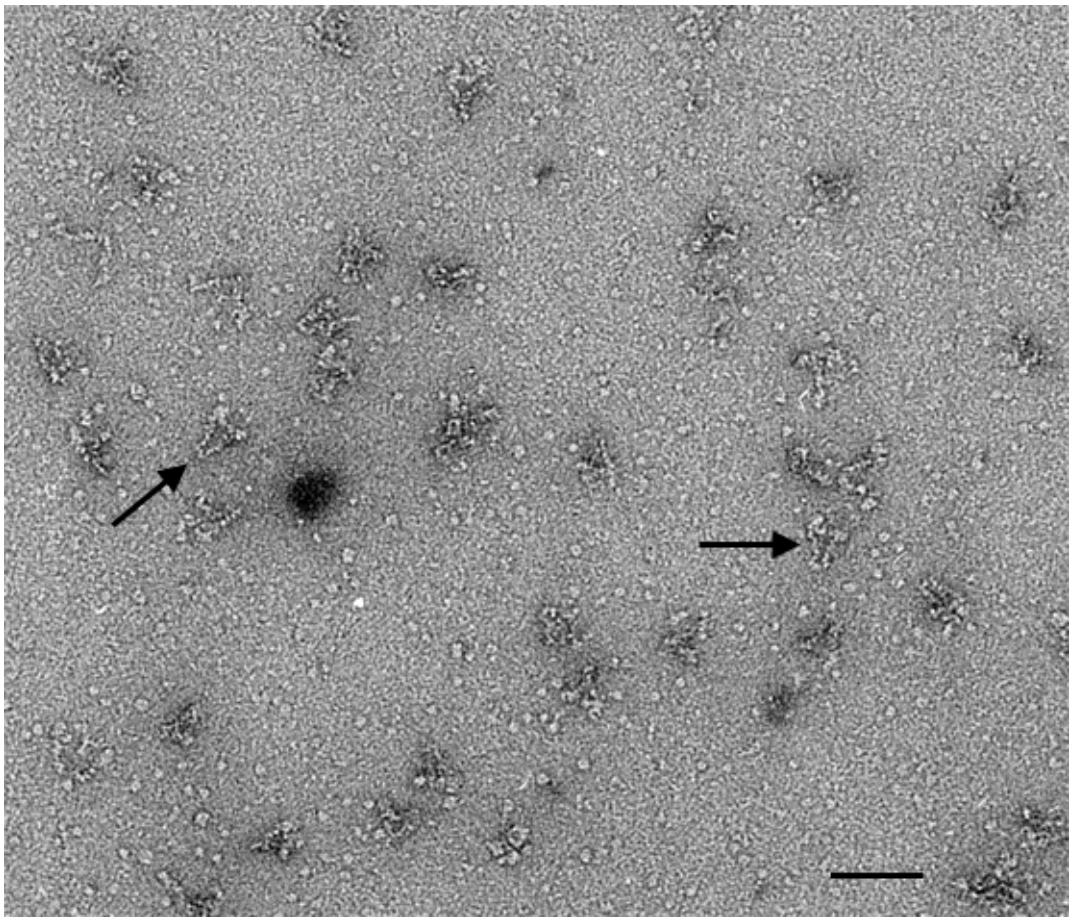

**Supplementary Figure 1. Field of myosin 5 molecules negative stained in ATP at nanomolar calcium.** Appearances are diverse, but a triangular morphology is common. Arrows indicate two particularly clear examples. Scale bar is 50 nm.

```
            117                   137
Mm 5a       P-IYGEDIINAYSGQNMGDMDP
Hs 5a       P-IYGEDIINAYSGQNMGDMDP
Ss 5a       P-IYGEDIINAYSGQNMGDMDP
Gg 5a       P-IYGEDIINAYSGQNMGDMDP
Xl 5a       P-IYGTDIINAYSGQNMGDMDP
Dr 5a       P-IYGADIINAYSGQNMGDMDP
Mm 5b       P-IYGQDVIYAYSGQNMGDMDP
Hs 5b       P-IYGQDVIYAYSGQNMGDMDP
Dr 5b       H-IYGEEVINAYSGQNMGDMDP
Mm 5c       P-IYGDAIIHAYSGQNMGDMDP
Hs 5c       P-IYGDAIIHAYSGQNMGDMDP
Dr 5c       P-IYGDAVIHAYSGQNMGDLDP
Dm 5        P-LYGPSIIRAYRGHAMGDLEP
Sc MYO2     Q-LYTQDMIQAYAGKRRGELRP
Sc MYO4     H-LYSREMIQNYSSKRKDELEP

Hs 1β       Q-IYSRQHMERYRGVSFYEVPP
Hs 2sm      P-IYSEKIVDMYKGKKRHEMPP
Hs 6        PKIYSSEAIKSYQGKSLGTRPP
Hs 7a       S-IYSPEHIRQYTNKKIGEMPP
Hs 9b       P-IYNPKYVKMYENQQLGKLEP
```

**Supplementary Figure 2. Sequence alignments.** Amino acid residues 117-137 of mouse myosin 5a are aligned with a representative selection of homologous sequences from other organisms and myosins. Acidic residues highlighted in red. Mm, Mus musculus; Hs, Homo sapiens; Ss, Sus scrofa; Gg, Gallus gallus; Xl, Xenopus laevis; Dr, Danio rerio; Dm, Drosophila melanogaster; Sc, Saccharomyces cerevisiae.

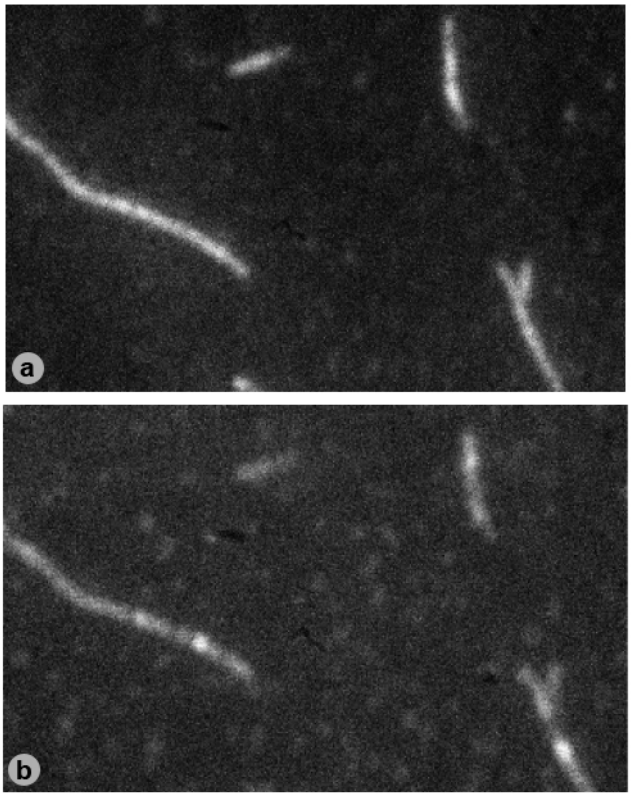


**Supplementary Figure 3. Decoration of actin filaments by a mixture of GFP-HMM and full length myosin.** Simultaneous visualisation by 2-colour TIRF microscopy of a mixture of (**a**) 1nM GFP-HMM and (**b**) 1nM Cy-3 labelled full length myosin binding to the same biotin-tethered actin filaments in the absence of ATP at nanomolar calcium. Both proteins decorate heavily. The lower intensity in the myosin image does not mean less binding, as it can arise from instrumental and optical differences between the two channels. Field of view is 15 µm x 9 µm.

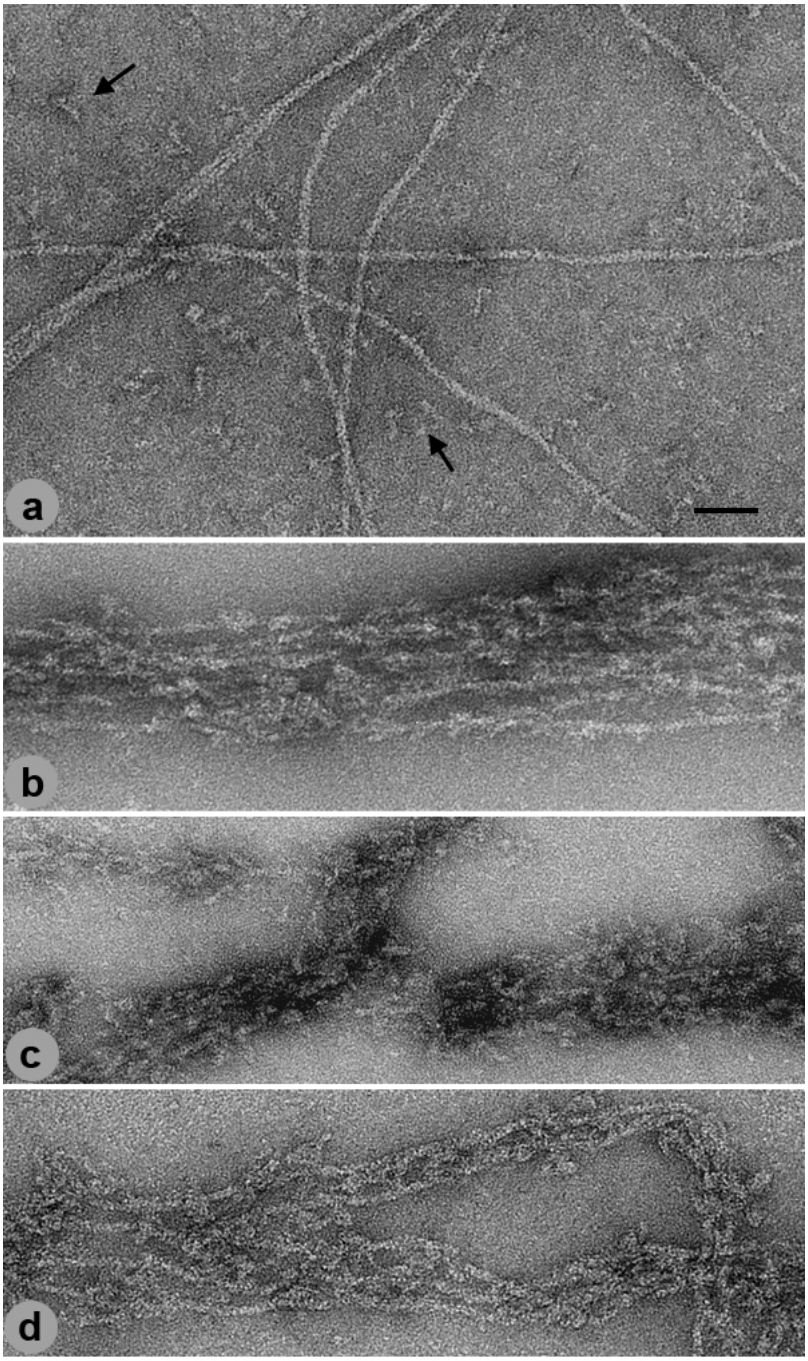


**Supplementary Figure 4. Fields of actin and myosin 5 mixtures with various nucleotides at nanomolar calcium, negative stained.** **a**, 1.25 mM ATP. Few if any myosins are attached to actin, so actin filaments can run close beside each other. Many folded myosins are seen in the background (two examples arrowed). **b**, 1.25 mM ADP, 25 mM phosphate. **c**, 1.25 mM ADP, no phosphate. **d**, no nucleotide or phosphate. **b-d** appear similar to each other, with most actin filaments and myosin molecules incorporated into bigger bundles than the ones shown, too heavily stained to decipher. Few myosin molecules are detached from actin. In the raft-like aggregates shown, the filaments are kept apart by myosin attaching between filaments. All experiments used 0.75 μM actin and 0.37 μM myosin 5.
Scale bar in **a** is 50 nm.

## 3 Supplementary Video Legends

**Full length myosin 5 is mostly inactive in solution at nanomolar calcium.** Simultaneous visualisation by 2-colour TIRF microscopy of 60pM GFP-HMM and 4000pM Cy-3 full length myosin interacting with biotin-tethered actin filaments in the presence of 1mM ATP and nanomolar calcium. The two movies of the same field of view were recorded simultaneously at 2 frames/s for 100s. They play at 30 frames/s *i.e.* 15x actual speed. Field of view is 15 μm x 9 μm. Despite the large molar excess of full length myosin over HMM, many fewer moving myosins are seen than HMMs.

**Supplementary Movie 1** GFP-HMM channel. (AVI 1.2MB)

**Supplementary Movie 2** Cy-3 whole myosin channel. (AVI 1.2MB)

## 4 Supplementary Methods

**Proteins.** Full length myosin 5a was purified from mouse brain[2], and labelled with Cy3-calmodulin[3]. Recombinant mouse myosin 5a HMM, N-terminal GFP-HMM, and S1 were expressed in the baculovirus/Sf9 system with calmodulin and purified as described[4] except that HMM was chromatographed on a mono-Q FPLC column using a 0.1-0.5M KCl gradient instead of the Q-Sepharose column. Actin and calmodulin were purified as previously described[2].

**Single molecule motility assay**. Single molecule TIRF assay was performed as described previously[3] in a buffer containing 50mM KCl, 4mM $MgCl_2$, ATP (1mM, 10μM or none), 0.1mM EGTA, 50mM dithiothreitol, 20mM MOPS, pH 7.5, and an oxygen scavenging system consisting of 2.5mg/ml glucose, 0.1mg/ml glucose oxidase, 2μg/ml catalase. The TIRF microscope setup was as described[3], except that a two colour observation system (Dual view system, Optical Insights, LLC, AL) was used to simultaneously view both GFP-HMM and Cy3-labeled myosin. It used a 565dcxr dichroic mirror, and emission filters (HQ510/20M for GFP and HQ640/50M for Cy3) in front of a cooled CCD camera (MicroMax BT, Roper). GFP-HMM and Cy3-myosin were added into a flow chamber in the presence of ATP and recorded at a frame rate of $2s^{-1}$. The number of moving spots on all actin filaments was counted in a $22x44\mu m^2$ area on both channels. Myosin concentration ranged from 60-4,000pM and HMM from 6-75pM.

**Electron microscopy and image processing.** Myosin 5 was incubated overnight in ice with calmodulin 1:12 M:M, then diluted and mixed with ATP to give 40nM myosin, 100mM KCl, 1.5mM $MgCl_2$, 20μM ATP, 0.1mM EGTA, 2mM Kphosphate, 10mM MOPS, pH 7.0 at 20°C. Within 5 min, 5μl were applied to a carbon-coated electron microscope grid and immediately stained with uranyl acetate[5]. Myosin was treated overnight with apyrase to produce nucleotide-free molecules. HMM-GTD complex was formed using 40nM HMM, 60nM GST-GTD dimer, 55μM ATP in the above buffer and stained as above. S1 was incubated with calmodulin 1:2 M:M and mixed with ATP to give 60nM S1, 2μM ATP, 25mM KCl, 2mM $MgCl_2$, 1mM EGTA, 20mM MOPS pH 7.0 at 20°C, and stained as above. Images were recorded on film at a nominal magnification of x40,000 using a JEOL1200EX at 80kV, and digitised at 0.52nm/pixel. Processing used the SPIDER suite as described[5], using K-means for classification and masks based on the variance in the global average. From a dataset of 1863 raw myosin images, classification into 90 classes yielded 17 classes containing 446 well-stained folded molecules. These were realigned and classified into 10 classes.

**Model building.** A model of the heavy chain of the lever as suggested by Houdusse et al.[6] was created using Swiss PDB Viewer software, using straight α-helix with the sequence of brush border myosin 1 for segments where the separation of IQ motifs is 23 residues, and the bent α-helix of scallop regulatory domain (1wdc.pdb) for separations of 25 residues. Calmodulin was superposed on the heavy chain using 1aji.pdb, superposing backbone atoms of 10 residues centred on the residues IQ on appropriate residues of the heavy chain model. Motor domains from myosin 5 ADP.$BeF_x$ (1w7j.pdb) or scallop myosin 2 ADP.Vi (1dfl.pdb) were added by superposing the proximal IQ motif of the myosin on the N-terminal IQ motif of the lever model then deleting the myosin levers. Residues up to Gly30 of the scallop motor domain were deleted, as structurally homologous sequence is absent from myosin 5.

## 5 Supplementary References


1. Burgess, S. *et al*. The prepower stroke conformation of myosin V. *J. Cell Biol*. **159**, 983-991 (2002).
2. Wang, F. *et al.* Regulated conformation of myosin V. *J. Biol. Chem*. **279**, 2333-2336 (2004).
3. Sakamoto, T. *et al*. Neck length and processivity of myosin V. *J. Biol. Chem*. **278**, 29201-29207 (2003).
4. Wang, F. *et al*. Effect of ADP and ionic strength on the kinetic and motile properties of recombinant mouse myosin V. *J. Biol. Chem*. **275**, 4329-4335 (2000).
5. Burgess, S. A., Walker, M. L., Thirumurugan, K., Trinick, J. & Knight, P. J. Use of negative stain and single-particle image processing to explore dynamic properties of flexible macromolecules. *J. Struct. Biol.* **147**, 247-258 (2004).
6. Houdusse, A., Silver, M. & Cohen, C. A model of $Ca^{2+}$-free calmodulin binding to unconventional myosins reveals how calmodulin acts as a regulatory switch. *Structure* **4**, 1475-1490 (1996).